Engineering Fracture Mechanics 78 (2011) 3243–3252

Contents lists available at SciVerse ScienceDirect

Engineering Fracture Mechanics

journal homepage: www.elsevier.com/locate/engfracmech

Compliance evolution in round cracked bars under tensile fatigue

J. Toribio [a,*], J.C. Matos [b], B. González [a], J. Escuadra [b]

[a] Department of Materials Engineering, University of Salamanca, E.P.S., Campus Viriato, Avda. Requejo 33, 49022 Zamora, Spain
[b] Department of Computing Engineering, University of Salamanca, E.P.S., Campus Viriato, Avda. Requejo 33, 49022 Zamora, Spain

ARTICLE INFO

Article history:
Received 1 February 2011
Received in revised form 4 August 2011
Accepted 14 September 2011

Keywords:
Dimensionless compliance
Fatigue crack growth
Numerical modelling
Cracked round bar
Paris law

ABSTRACT

This paper studies the dimensionless compliance in cylindrical geometries with transverse surface cracks subjected to axial tensile loading. Compliance evolution is analyzed when round bars are subjected to fatigue with free and constrained sample ends, initial crack geometries of straight or circular fronts and several materials characterized through of the Paris parameter *m*. With this aim, a computer application that calculates the crack front's geometric evolution and the dimensionless compliance was made by discretizing the crack front and assuming that every point advance perpendicular to the crack front according to the Paris law. The results show that dimensionless compliance grows with the increase of the relative crack depth and the decrease of the aspect ratio, showing greater values for free sample ends than for constrained sample ends. Furthermore, during fatigue crack growth, materials with higher values of the Paris parameter *m* produce slightly greater dimensionless compliance and a better convergence between the results for straight or circular initial crack.

1. Introduction

The problem of fatigue crack propagation in cylindrical geometries is of great interest in fracture mechanics, because it is one of the most common geometries in linear structural elements. These components, usually subjected to oscillating load, may fracture, generally, after surface fatigue crack growth, with semi-elliptical shapes contained in a plane perpendicular to the loading axis.

Several criteria have been stated in the past to characterize fatigue crack growth in these geometries, e.g., prediction of the 90° intersecting angle of the crack with the surface or the iso-*K* criterion along the crack front [1]. The most used being that based on the Paris Erdogan law [2–7], which requires the knowledge of the dimensionless stress intensity factor (SIF), *Y*, along the crack front in the round cracked bar. It has been deducted by several authors following different procedures: compliance methods, finite element analysis, boundary integral equation methods, experimental techniques, etc. [1,8–10].

Dimensionless compliance in round cracked bars under tension or bending depends on the crack geometry. If the crack is characterized by an elliptical shape, there are two factors exerting influence: the relative crack depth (crack depth divided by the diameter), which causes an increase of its value, and the aspect ratio (ratio between the crack depth and the other semi-axis of the ellipse), which causes a decrease of its value [3,11]. Thus, there is a relation between the change in compliance during fatigue crack growth and the crack geometry evolution, which depends on the specimen material, the initial crack geometry and the type of applied load [7,12].

Experimentally the geometrical evolution of the crack front in a cylindrical bar can just be observed *post mortem* (once fractured) and there are several techniques to mark the front according to the material studied. It is possible to relate the

* Corresponding author. Tel.: +34 980 54 50 00; fax: +34 980 54 50 02.
E-mail address: toribio@usal.es (J. Toribio).

0013-7944/$ - see front matter © 2011 Elsevier Ltd. All rights reserved.
doi:10.1016/j.engfracmech.2011.09.013

crack front geometry with compliance, one of the few characteristics which can be measured during the crack propagation. The aim of this paper is to obtain the dimensionless compliance in cracked cylindrical bars subjected to tension with different crack geometries (crack depths and aspect ratios), as well as analyzing how dimensionless compliance evolves when fatiguing round bars of different materials (coefficient m of Paris 2, 3 and 4), with different initial crack geometries (circular and quasi-straight, both crack shapes with relative depth a/D of 0.1, 0.3 and 0.5) and applying tensile load to round bars with free sample ends and constrained sample ends.

2. Numerical modelling

A computer program in the Java programming language was developed to determine the geometrical evolution of the crack front according to the Paris law, for transverse surface crack in cylindrical geometries subjected to tensile fatigue load, which would be the basis to determine the change which occurs in the dimensionless compliance of the round bar.

2.1. Fatigue crack front evolution

The basic hypothesis of the modelling consisted of assuming that the crack front can be modelled as an ellipse with centre on the bar surface [13] and the fatigue propagation takes place in a direction perpendicular to this crack front, following the really sound (and the most widely accepted) crack growth criterion: the Paris Erdogan law [14],

$$\frac{da}{dN} = C\Delta K^m \tag{1}$$

Every elliptical arc of the crack front was divided in 14 segments with exactly the same length using the Simpson's rule in order to discretize the front. The point on the round bar surface was not taken into account, since it presents some difficulties regarding the computation of the dimensionless SIF (there is a plane stress state on the crack surface). After that, every single point was shifted according to Paris Erdogan law perpendicular to the front and so as to keep constant the maximum crack depth increment, $\Delta a(\max) \equiv \max \Delta a_i = D/1000$, all over the process [15]. The advance of every front point, Δa_i, can be obtained from the maximum crack increment and the ratio of the dimensionless SIF,

$$\Delta a_i = \Delta a(\max)\left[\frac{Y_i}{Y(\max)}\right]^m \tag{2}$$

The newly obtained points, fitted by the least squares method [13], generate a new ellipse with which the process is repeated iteratively until the desired crack depth is reached. Due to the existing symmetry, only half the problem was used for the computations (Fig. 1).

The dimensionless SIF, Y, is three-parametric for the crack modelled as an ellipse with centre on the round bar surface and its value depends on the crack geometry and on the point on the front where it is calculated. The dimensionless SIF used in the computations is that proposed by Shin and Cai [10] obtained by the finite element method and the virtual crack extension technique, whose value is function of the relative crack depth a/D, the aspect ratio a/b, and the position of the point considered on its front x/h (Fig. 2).

The fitting of the results provides a three-parametrical expression which is defined as a function of the coefficients M_{ijk} (Table 1), which are different depending on tension with free sample ends or constrained sample ends,

$$Y = \sum_{i=0}^{2}\sum_{j=0}^{7}\sum_{k=0}^{2} M_{ijk}\left(\frac{a}{b}\right)^i\left(\frac{a}{D}\right)^j\left(\frac{x}{h}\right)^k \tag{3}$$

2.2. Dimensionless compliance

If tensile load is applied, it is obtained that the local displacement u is related to the applied force F through compliance as follows:

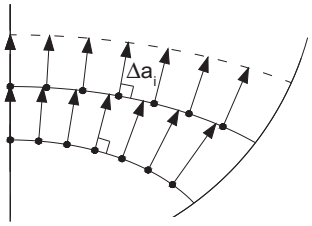

Fig. 1. Process followed to compute the fatigue crack growth.

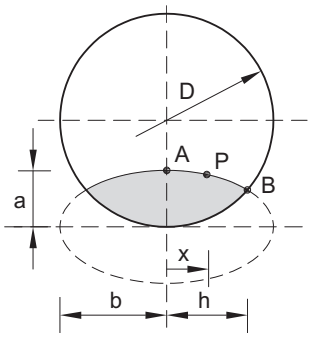

Fig. 2. Crack characterization.

Table 1
SIF coefficients M_{ijk} for tension proposed by Shin and Cai [10].

i	j	$k=0$	$k=1$	$k=2$
(a) Free sample ends, i.e., unrestrained bending				
0	0	0.220	0.123	−0.409
0	1	28.513	0.511	−9.764
0	2	−354.782	−2.034	128.817
0	3	2178.632	−19.569	−727.078
0	4	−7140.202	144.435	2201.067
0	5	12957.447	−359.284	−3732.813
0	6	−12227.977	393.518	3343.521
0	7	4721.868	−159.206	−1240.214
1	0	−0.326	0.065	1.011
1	1	−3.780	−6.878	−3.946
1	2	79.489	47.747	41.099
1	3	−571.094	−119.954	−316.682
1	4	1976.255	14.769	1284.860
1	5	−3583.421	423.169	−2563.292
1	6	3256.770	−661.610	2455.158
1	7	−1163.158	306.176	−880.302
2	0	0.266	0.118	−1.584
2	1	−9.118	−3.515	45.562
2	2	85.381	75.016	−552.891
2	3	−465.013	−587.594	3322.477
2	4	1475.911	2197.404	−10812.317
2	5	−2794.532	−4264.810	19328.127
2	6	2878.868	4138.287	−17829.715
2	7	−1261.348	−1588.135	6638.698
(b) Constrained sample ends, i.e., restrained bending				
0	0	1.095	0.113	−0.896
0	1	−1.336	1.824	3.092
0	2	13.108	−21.709	−4.197
0	3	−43.689	105.483	−13.255
0	4	134.868	−271.225	51.548
0	5	−242.653	387.470	−59.329
0	6	254.093	−290.024	13.481
0	7	−108.196	88.387	10.854
1	0	−1.177	0.271	0.904
1	1	17.924	−11.649	0.701
1	2	−137.252	98.358	−32.641
1	3	545.816	−415.027	204.104
1	4	−1223.334	982.713	−568.407
1	5	1541.587	−1329.634	857.543
1	6	−1006.656	961.893	−657.659
1	7	264.206	−288.565	191.570
2	0	0.725	−0.388	0.008
2	1	−17.427	10.074	−4.883
2	2	134.652	−80.088	55.092
2	3	−551.902	328.165	−305.079
2	4	1239.493	−772.921	916.962
2	5	−1548.537	1055.952	−1545.428
2	6	969.388	−784.581	1372.595
2	7	−227.132	245.798	−485.556

$$u = \lambda F \tag{4}$$

The strain energy density U can be expressed taking into account the equivalence between the energy release rate G and the stress intensity factor in plane strain K,

$$\mathrm{d}U = G\mathrm{d}A = \frac{K^2(1-\nu^2)}{E}\mathrm{d}A \tag{5}$$

where ν is the Poisson coefficient and $\mathrm{d}A$ the differential of the crack area. On the other hand, the strain energy density for a cracked bar subjected to tensile load is, introducing the value $\mathrm{d}u$ from the Eq. (4),

$$\mathrm{d}U = \frac{1}{2}F\mathrm{d}u = \frac{1}{2}F^2\mathrm{d}\lambda \tag{6}$$

The stress intensity factor in plane strain for the geometry of the study can be obtained as follows:

$$K = Y\sigma\sqrt{\pi a} \tag{7}$$

where the stress σ for axial tension is calculated:

$$\sigma = \frac{4F}{\pi D^2} \tag{8}$$

If Eqs. (5) and (6) for strain energy density are made equal and introducing values K (Eq. (7)) and σ (Eq. (8)), the following expression is obtained:

$$\frac{1}{2}F^2\mathrm{d}\lambda = \left[Y\frac{4F}{\pi D^2}\sqrt{\pi a}\right]^2\frac{(1-\nu^2)}{E}\mathrm{d}A \tag{9}$$

and isolating compliance in the Eq. (9), it is obtained:

$$\lambda = \frac{32(1-\nu^2)}{\pi D^4 E}\int_0^a Y^2 a\mathrm{d}A \tag{10}$$

Solving the integral which appears in Eq. (10) is not trivial. In order to achieve that, the Cartesian coordinates (x, y) were change into parametrical coordinates (a, θ), relating themselves both through the expressions:

$$x = b\cos\theta \tag{11}$$

$$y = a\sin\theta \tag{12}$$

where the correspondence between angles δ and θ, deducted from Fig. 3, is as follows,

$$\tan\delta = \frac{y}{x} = \frac{a}{b}\tan\theta \tag{13}$$

The differential of the ellipse area modelling the crack advance is:

$$\mathrm{d}A = \mathrm{d}x \wedge \mathrm{d}y \tag{14}$$

differentiating the coordinates (x,y) according to the new coordinates (a,θ),

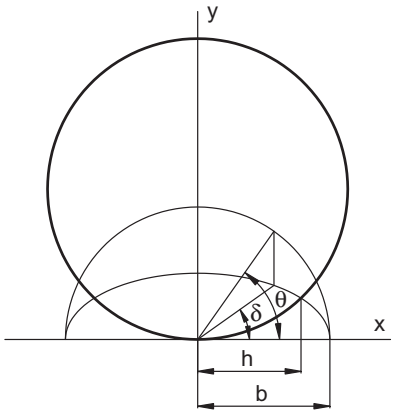

Fig. 3. Relationship between δ and θ angles.

$$dx = b'(a)\cos\theta\,da - b\sin\theta\,d\theta \tag{15}$$

$$dy = \sin\theta\,da + a\cos\theta\,d\theta \tag{16}$$

and substituting these expressions on the Eq. (14), it is obtained,

$$dA = (ab'(a)\cos^2\theta + b\sin^2\theta)\,da \wedge d\theta \tag{17}$$

The problem that arises in calculating Eq. (17) can be found in the previous knowledge of the variation of the parameter b with the crack depth a. The definition of the derivative at a point can be used to this purpose,

$$b'(a) \approx \frac{b(a+\Delta a) - b(a)}{\Delta a} \tag{18}$$

Introducing Eq. (17) in Eq. (10), which allows calculating compliance in a cracked round bar subjected to axial tensile loading, it is obtained:

$$\lambda = \frac{64(1-\nu^2)}{\pi D^4 E}\int_0^a \int_{\arccos\frac{h}{b}}^{\pi/2} Y^2 a(ab'(a)\cos^2\theta + b\sin^2\theta)\,d\theta\,da \tag{19}$$

where f is defined as the *dimensionless compliance* due to tensile load,

$$f = \int_0^a \int_{\arccos\frac{h}{b}}^{\pi/2} Y^2 \frac{a}{D^3}(ab'(a)\cos^2\theta + b\sin^2\theta)\,d\theta\,da \tag{20}$$

There is an easier way to obtain the differential of the area of the ellipse which models the crack advance, which consists of approximating this calculation by using the following expression:

$$dA \approx 2S\,da \tag{21}$$

where $2S$ is the arc length of the crack front which is expressed in parametric coordinates as follows,

$$S = \int_{\theta_0}^{\theta_1} \sqrt{(x'(\theta))^2 + (y'(\theta))^2}\,d\theta = \int_{\arccos\frac{h}{b}}^{\pi/2} a\sqrt{\left(\frac{b}{a}\right)^2 \sin^2\theta + \cos^2\theta}\,d\theta \tag{22}$$

and substituting in Eq. (10),

$$\lambda \approx \frac{64(1-\nu^2)}{\pi D^4 E}\int_0^a \int_{\arccos\frac{h}{b}}^{\pi/2} Y^2 a^2 \sqrt{\left(\frac{b}{a}\right)^2 \sin^2\theta + \cos^2\theta}\,d\theta\,da \tag{23}$$

an approximate expression of the dimensionless compliance, f, is obtained:

$$f \approx \int_0^a \int_{\arccos\frac{h}{b}}^{\pi/2} Y^2 \frac{a^2}{D^3}\sqrt{\left(\frac{b}{a}\right)^2 \sin^2\theta + \cos^2\theta}\,d\theta\,da \tag{24}$$

The dimensionless compliance value can be calculated incrementally with the crack growth, where the integral,

$$f = \sum_i \int_{a_i}^{a_{i+1}} \int_{\arccos\frac{h}{b}}^{\pi/2} R\,d\theta\,da \tag{25}$$

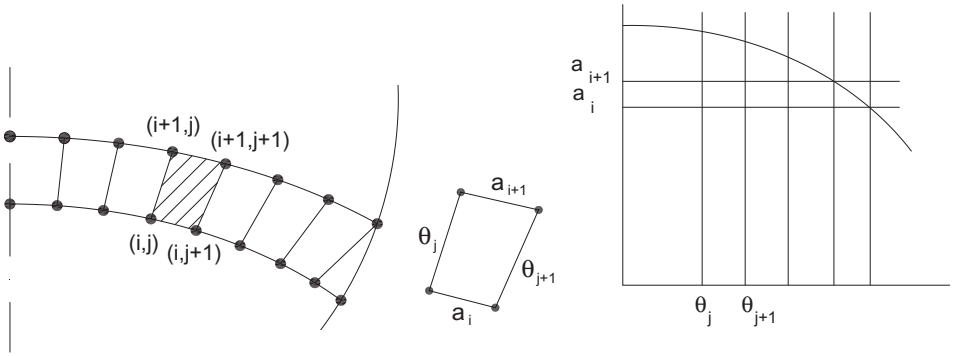

Fig. 4. Divisions with the isolines used in the trapezoidal rule.

it is solved using the trapezoidal rule (where R is the corresponding expression according to Eq. (20) or Eq. (24)), following the scheme on Fig. 4, dividing every crack increment in eight parts for half of the problem, so they correspond with the coordinate's isolines (a, θ).

The compliance increment in every crack advance is calculated using the following expression,

$$f = \sum_i (a_{i+1} - a_i) \left(\sum_{j=0}^{7} (\theta_{j+1} - \theta_j) \frac{(R(i,j) + R(i,j+1) + R(i+1,j) + R(i+1,j+1))}{4} + \frac{(\theta_8 - \theta_7)}{2} \frac{(R(i,7) + R(i+1,7) + R(i,8))}{3} \right) \tag{26}$$

In the results shown, Eq. (20) and not Eq. (24) has been used for calculating the dimensionless compliance, because there were disagreements of up to 15% between the two solutions (Eq. (20) does not approximate the element of the area, whereas Eq. (24) does). In order to obtain the dimensionless compliance of the initial crack, the process is similar to the one just described, but easier, because it considers that every previous crack front has the same aspect ratio as the initial one. Furthermore, compliance due to smaller cracks than the minimum ones considered by Shin and Cai (a/D = 0.067) were not taken into account.

3. Numerical results and discussion

In cracked cylindrical bars with tensile load, dimensionless compliance f depends on the restriction on the specimen ends, on relative crack depth a/D and on the aspect ratio a/b. Figs. 5 and 6 show how dimensionless compliance varies with these parameters. It can be observed how dimensionless compliance increases when so does relative crack depth. For a given depth, dimensionless compliance decreases with the aspect ratio, from quasi-straight front cracks (a/b = 0.08) to completely circular ones (a/b = 1.00). Hence, there is a strong dependency between dimensionless compliance and aspect ratio. Furthermore, dimensionless compliance is much greater under tension with free sample ends (Fig. 5) than under tension with constrained sample ends (Fig. 6), increasing the difference between both results with relative crack depth and with the aspect ratio.

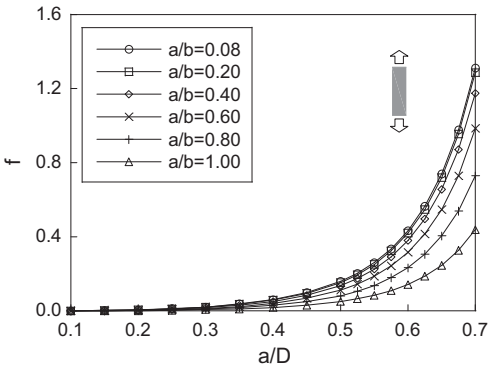

Fig. 5. Dimensionless compliance (free sample ends).

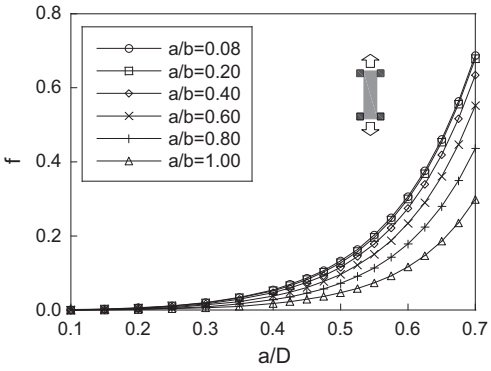

Fig. 6. Dimensionless compliance (constrained sample ends).

With regard to dimensionless compliance, a comparative study was carried out of the results of this modelling and those obtained by other authors, which present round bars subject to tension with free sample ends from certain crack geometries, $a/D \leqslant 0.6$ and $a/b = \{0.08, 0.20, 0.40, 0.60, 0.80, 1.00\}$ (Fig. 7). Shih and Chen [3] estimated dimensionless compliance using the mean value of the two expressions of the dimensionless SIF obtained by Carpinteri [9] for that calculation. Rubio et al. [11] considered the variation of the dimensionless SIF along the crack front with the expression of Shin and Cai, using the trapezoidal rule in order to calculate the integral of the compliance with an approximate value of the element of area (Eqs. (21) and (24)). In this study, compliance has also been obtained using the Shin and Cai expressions along the crack front, where the integral was calculated *without approximating the element of area* (Eqs. (17) and (20)), using the trapezoidal rule with elements of area small enough, as was supported by a previous convergence study.

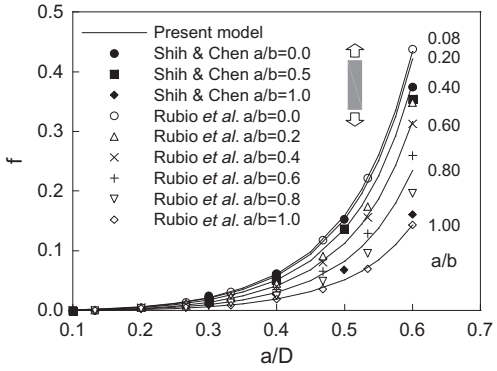

Fig. 7. Comparison between prediction of the presents model and results from other researchers (free sample ends).

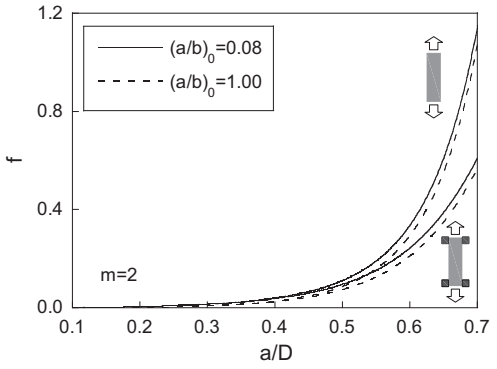

Fig. 8. Dimensionless compliance ($m = 2$ and $(a/D)_0 = 0.1$).

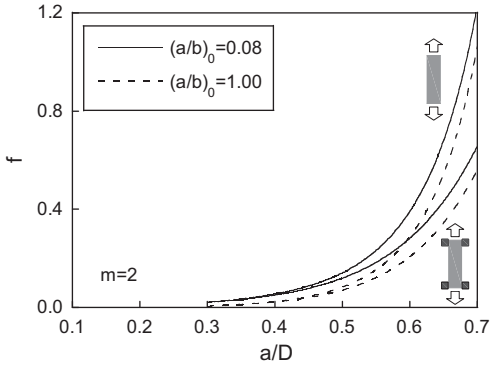

Fig. 9. Dimensionless compliance ($m = 2$ and $(a/D)_0 = 0.3$).

The values of Shih and Chen for $a/b = 0.0$ coincide to a great extent with the results of the present model for $a/b = 0.08$, the first being slightly inferior in the section $a/D = 0.5$–0.6. For $a/b = 0.5$ and 1.0 the results of Shih and Chen have a very similar tendency, but with slightly higher values. Rubio et al. show a great coincidence for $a/b = 0.0$ and 1.0, remaining the rest of the curves for constant a/b approximately equidistant (except for $a/b = 0.2$ which is closer to $a/b = 0.4$ than to $a/b = 0.0$), whereas in this paper the representations for constant a/b are closer one to another as the crack front gets straighter, and therefore, the values of Rubio et al. are below.

The dimensionless compliance evolution during fatigue crack propagation is shown on Figs. 8–16, for initial crack depths $(a/D)_0 = \{0.1, 0.3, 0.5\}$, initial aspect ratios $(a/b)_0 = 0.08$ (quasi-straight crack front) and $(a/b)_0 = 1.00$ (circular crack front), different materials (Paris exponent m 2, 3 and 4) and tensile load with free sample ends and constrained sample ends. The chosen initial aspect ratios (quasi-straight and circular) represent the two limit cases of the wide set of possible initial

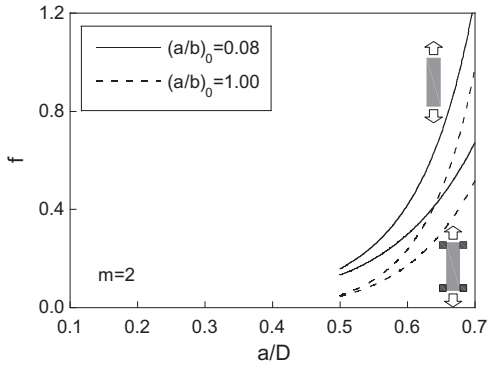

Fig. 10. Dimensionless compliance ($m = 2$ and $(a/D)_0 = 0.5$).

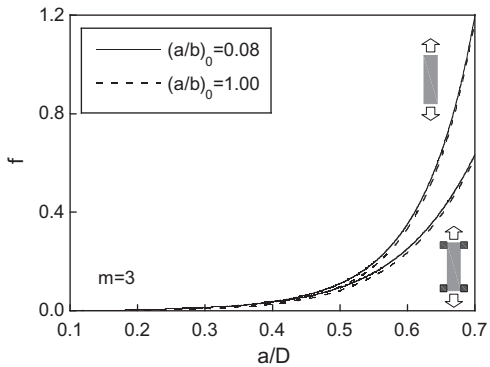

Fig. 11. Dimensionless compliance ($m = 3$ and $(a/D)_0 = 0.1$).

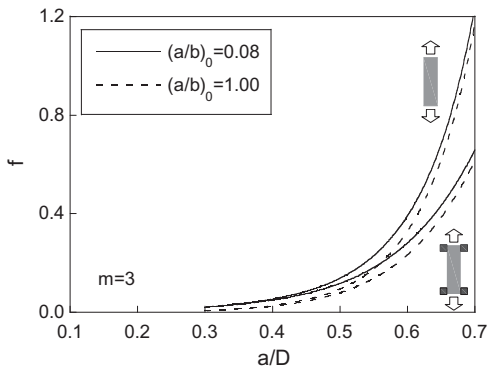

Fig. 12. Dimensionless compliance ($m = 3$ and $(a/D)_0 = 0.3$).

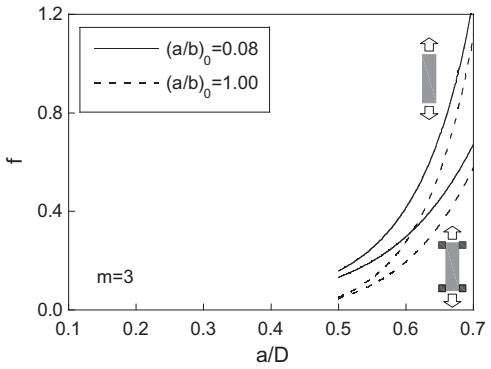

Fig. 13. Dimensionless compliance ($m = 3$ and $(a/D)_0 = 0.5$).

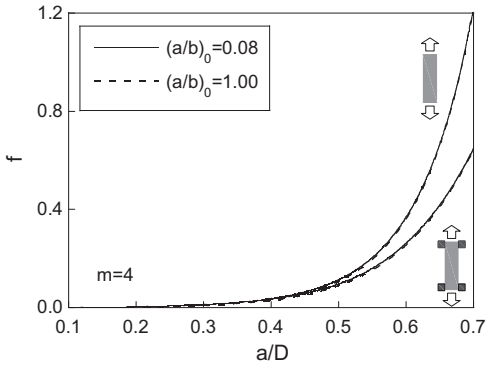

Fig. 14. Dimensionless compliance ($m = 4$ and $(a/D)_0 = 0.1$).

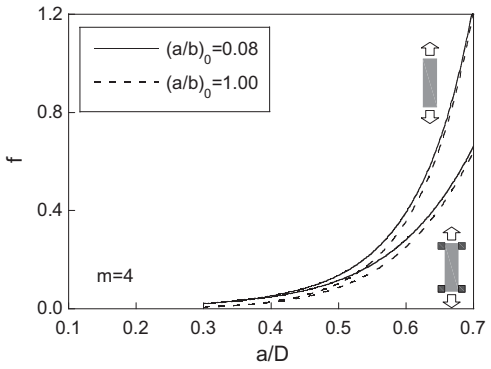

Fig. 15. Dimensionless compliance ($m = 4$ and $(a/D)_0 = 0.3$).

crack shapes. Their evolution under fatigue loading shows that any starting crack evolves towards an elliptically-shaped flaw after certain number of cycles.

During crack growth, it can observed how dimensionless compliance presents a great dependency with relative crack depth (which makes it to increase), and that the aspect ratio (which makes it decrease) influences to a lesser extent, because of the strong geometrical convergence produced during fatigue crack growth [12,15]. Furthermore, the convergence of results for both initial crack fronts, quasi-straight and circular, is greater for smaller initial crack depths.

The dimensionless compliance in initial cracks with a quasi-straight front doubles that of those with a circular front, although both are very small, increasing with growth at the same time as their values tend to be equal. In crack propagation, the dimensionless compliance values, up to approximately a crack depth of half the specimen, are similar for both conditions on the specimen ends (free and constrained), from whose size the dimensionless compliance for free sample ends increases

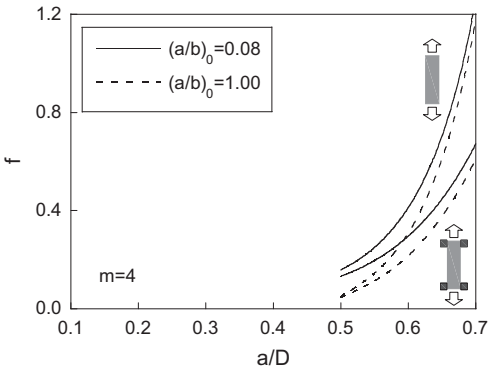

Fig. 16. Dimensionless compliance ($m = 4$ and $(a/D)_0 = 0.5$).

more than for constrained sample ends (reaching a value which almost doubles for a depth of $0.7D$). Furthermore, dimensionless compliance curves present a greater convergence for free sample ends than for constrained ones.

The increase of the parameter m, Paris exponent of the material, offers slightly higher values of dimensionless compliance for an circular initial front $(a/b)_0 = 1$, and it is almost the same for a quasi-straight initial front $(a/b)_0 = 0.08$. It is also observed how the greater the coefficient m (characteristic of the material), the greater the convergence between results for the different initial geometries. The difference between results for the different values of m is always bigger between $m = 2$ and $m = 3$ than between $m = 3$ and $m = 4$, which implies that as this parameter increases, the results depend less on it.

4. Conclusions

Dimensionless compliance f increases with relative crack depth a/D and decreases with the aspect ratio a/b, so that the representations f-a/D for constant a/b are closer one to another as the aspect ratio gets smaller (straighter crack front). Furthermore, the dimensionless compliance for tensile load with free sample ends is greater than for constrained sample ends and the difference increases with relative crack depth as well as with the decrease of the aspect ratio.

In fatigue crack propagation, relative crack depth influences more on dimensionless compliance than the aspect ratio, because the crack front tends to converge when the crack propagates from different initial geometries.

In fatigue crack growth, dimensionless compliance is greater under tension with free sample ends than with constrained sample ends, increasing the difference between its values with relative crack depth and obtaining for $a = 0.7D$ a dimensionless compliance value almost twice as high in free sample ends as in constrained sample ends.

The increase of the Paris exponent m offers slightly higher values of dimensionless compliance (more for circular initial crack front $(a/b)_0 = 1$ than for quasi-straight initial crack front $(a/b)_0 = 0.08$). Furthermore, as m increases, a greater convergence is also produced in values of dimensionless compliance for the different initial crack conditions.

Acknowledgements

The authors wish to acknowledge the financial support provided by the following Spanish Institutions: Ministry for Science and Technology (MCYT; Grant MAT2002-01831), Ministry for Education and Science (MEC; Grant BIA2005-08965), Ministry for Science and Innovation (MICINN; Grant BIA2008-06810) and *Junta de Castilla y León* (JCyL; Grants SA067A05, SA111A07 and SA039A08).

References

[1] Levan A, Royer J. Part-circular surface cracks in round bars under tension, bending and twisting. Int J Fract 1993;61(1):71–99.
[2] Carpinteri A. Shape change of surface cracks in round bars under cyclic axial loading. Int J Fatigue 1993;15(1):21–6.
[3] Shih Y-S, Chen J-J. Analysis of fatigue crack growth on a cracked shaft. Int J Fatigue 1997;19(6):477–85.
[4] Couroneau N, Royer J. Simplified model for the fatigue growth analysis of surface cracks in round bars under mode I. Int J Fatigue 1998;20(10):711–8.
[5] Lin XB, Smith RA. Shape growth simulation of surface cracks in tension fatigued round bars. Int J Fatigue 1997;19(6):461–9.
[6] Lin XB, Smith RA. Fatigue growth simulation for cracks in notched and unnotched round bars. Int J Mech Sci 1998;40(5):405–19.
[7] Shin CS, Cai CQ. Evaluating fatigue crack propagation properties using a cylindrical rod specimen. Int J Fatigue 2007;29(3):397–405.
[8] Astiz MA. An incompatible singular elastic element for two- and three-dimensional crack problems. Int J Fract 1986;31(2):105–24.
[9] Carpinteri A. Elliptical-arc surface cracks in round bars. Fatigue Fract Engng Mater Struct 1992;15(11):1141–53.
[10] Shin CS, Cai CQ. Experimental and finite element analyses on stress intensity factors of an elliptical surface crack in a circular shaft under tension and bending. Int J Fract 2004;129(3):239–64.
[11] Rubio L, Muñoz-Abella B, Loaiza G. Static behaviour of a shaft with an elliptical crack. Mech Syst Sig Process 2011;25:1674–86.
[12] Toribio J, González B, Matos JC. Fatigue crack propagation in cold drawn steel. Mater Sci Engng A 2007;468–470:267–72.
[13] Toribio J, Matos JC, González B, Escuadra J. An automated procedure for the geometrical modelling of a surface crack front. Struct Durab Health Monit 2009;123(1):1–16.
[14] Paris PC, Erdogan F. A critical analysis of crack propagation laws. J Basic Engng 1963;85D:528–34.
[15] Toribio J, Matos JC, González B, Escuadra J. Numerical modelling of crack shape evolution for surface flaws in round bars under tensile loading. Engng Fail Anal 2009;16(2):618–30.